CITATION

Di Iorio, D., J.W. Lavelle, P.A. Rona, K. Bemis, G. Xu, L.N. Germanovich, R.P. Lowell, and G. Genc. 2012. Measurements and models of heat flux and plumes from hydrothermal discharges near the deep seafloor. *Oceanography* 25(1):168–179, http://dx.doi.org/10.5670/oceanog.2012.14.

DOI

http://dx.doi.org/10.5670/oceanog.2012.14

COPYRIGHT

USAGE

Measurements and Models of Heat Flux and Plumes

from Hydrothermal Discharges Near the Deep Seafloor

BY DANIELA DI IORIO, J. WILLIAM LAVELLE, PETER A. RONA, KAREN BEMIS,

GUANGYU XU, LEONID N. GERMANOVICH, ROBERT P. LOWELL, AND GENCE GENC

White flocculent bacterial mats in and around extremely gassy high-temperature (> 100°C) white smokers at the Champagne vent site, Mariana island arc region, western Pacific Ocean. Photo credit: *Pacific Ring of Fire 2004 Expedition; NOAA Office of Ocean Exploration; Dr. Bob Embley, NOAA PMEL, Chief Scientist*

ABSTRACT. Deep-sea hydrothermal vents are conduits of heat and chemicals from the lithosphere to the hydrosphere. Their plumes rise hundreds of meters from the seafloor into the water column; during their ascent, they entrain ambient water and are subject to cross flows. Source fluxes can vary in time, partly in response to seismic and magmatic events. Long-term measurements of physical properties of hydrothermal plumes provide windows to conditions within Earth's interior. This article provides examples of long-term measurements of acoustic scattering recorded along Endeavour Segment of the Juan de Fuca Ridge. Acoustic *backscatter* data from particles and temperature fluctuations provide information on width, shape, and vertical velocity in the plumes from which entrainment and upward transport are estimated. Acoustic *forward scatter* by turbulence within the plume gives time series of the plume's path-averaged vertical velocity and temperature fluctuations and exhibits variability that is dependent on the ambient horizontal flow. At several vents, direct measurements of heat flux using in situ devices and video imagery have yielded an integrated heat output for various sulfide structures. In conjunction with these measurements, plume models that incorporate ambient stratification and horizontal tidal flows are yielding insights into the vertical and azimuthal dependence of entrainment, rise-height variability, and plume bending.

INTRODUCTION

Since their discovery in the late 1970s, deep-sea hydrothermal vents have been of interest to marine geologists, geophysicists, and biogeochemists because of their potential for providing information on conditions beneath the seafloor and because biogeochemically reactive materials like sulfide and reduced metals are transported to the ocean. One long-term goal in studying these systems is to quantify the contributions hydrothermal fluids make to the chemical and thermal budget of the global ocean. A more achievable short-term goal is to quantify the heat flux from a single vent or an ensemble of vents (i.e., a vent field, though even that task is not simple). Quantification is difficult because of the large variety of source fluxes, from relatively warm to very hot and, in some cases, their time-variable nature, as well as the moving environment into which the discharge is injected, the small size of vent orifices, the spacing irregularity between individual vents in a vent field,

and, of course, their deep ocean location.

Hydrothermal fluids issue from chimney-like structures formed from the precipitation of metals extracted from the subseafloor by ocean water circulating downward into the crust and heated to high temperatures (Tivey, 2007). Highest temperatures are usually found in the chimney discharge. When these high-temperature, chemical-laden fluids mix with cold ambient ocean water, they form metallic sulfides, oxihydroxides, and sulfates. These precipitating minerals give the effluent a black (and sometimes a gray or white) smoke look. These "black smoker" chimneys often discharge as forced jets with velocities up to meters per second and temperatures up to about 400°C. The chimneys are typically meters high and have internal diameters on the order of 10 cm. Plumes of buoyant chimney effluents rise up to hundreds of meters above the seafloor as a consequence of density deficiency produced by their differences in temperature and salinity from those of the surrounding seawater (Turner and Campbell, 1987; Speer and Rona, 1989). In some cases, these discharges have built large (25–100 m^2) sulfide mounds on which a handful of chimneys, at seemingly random sites, may be perched.

In contrast, diffuse fluids, which are generally mixtures within the subsurface of cold seawater and either magmatically heated fluids or conductively heated seawater (see Bemis et al., 2012, in this issue for a review), typically exhibit temperatures of degrees to tens of degrees Celsius with vertical flow velocities up to tens of centimeters per second. The diffuse fluids lack the buoyancy to rise more than a few tens

Daniela Di Iorio (daniela@uga.edu) is Associate Professor, Department of Marine Sciences, University of Georgia, Athens GA, USA. **J. William Lavelle** is Physical Oceanographer, National Oceanic and Atmospheric Administration Pacific Marine Environmental Laboratory, Seattle, WA, USA. **Peter A. Rona** is Professor, Institute of Marine and Coastal Sciences, Rutgers University, New Brunswick, NJ, USA. **Karen Bemis** is Research Associate, Institute of Marine and Coastal Sciences, Rutgers University, New Brunswick, NJ, USA. **Guangyu Xu** earned a master's degree from the Department of Marine Sciences, University of Georgia, Athens, GA, USA, and is currently a PhD candidate in the Institute of Marine and Coastal Sciences, Rutgers University, New Brunswick, NJ, USA. **Leonid N. Germanovich** is Professor, School of Civil and Environmental Engineering, Georgia Institute of Technology, Atlanta, GA, USA. **Robert P. Lowell** is Research Professor, Department of Geosciences, Virginia Tech, Blacksburg, VA, USA. **Gence Genc** is PhD Candidate, School of Civil and Environmental Engineering, Georgia Institute of Technology, Atlanta, GA, USA.

of meters off the seafloor but can be entrained by black smoker plumes (Lavelle and Wetzler, 1999). The diffuse fluids are typically clear, and, as a result, an observer can see refraction effects similar to those created by hot air rising from an asphalt road on a hot day. This phenomenon may be visible over areas up to square meters and within meters of seafloor that is illuminated by submerged vehicle floodlights.

Unlike either of the other flow regimes, flow from beneath chimney flanges, which are lateral outgrowths from a supporting sulfide mound, may attain the high temperatures of black smokers, but their effluent is clear (Woods and Delaney, 1992). The flow precipitates metals at the leading edges of the flanges, typically of the order of 1 m in diameter, that grow outward as the flow mixes with seawater. Pools of high-temperature water (up to 350°C) can form beneath the flanges (see Figures 4 and 5 in Tivey, 2007).

Measuring heat flux from hydro-thermal vents is by no means an easy task, and measurements have been carried out in a variety of ways. One approach is to measure the heat flux at individual vents directly and then sum up the results to extrapolate the heat flux from a hydrothermal edifice or even an entire vent field (e.g., Schultz et al., 1992; Bemis et al., 1993; Ginster and Mottl, 1994). Another way to measure the heat flux is to survey the water column at the equilibrium layer, where hydrothermal plumes reach neutral buoyancy with respect to the ambient seawater (e.g., Baker and Massoth, 1987; Rosenberg et al., 1988; Thomson et al., 1992). A third approach is to set up a control volume enclosing a hydro-thermal edifice or an entire vent field and measure the net heat flux leaking through the boundaries of the control volume (Stahr et al., 2000; Veirs et al., 2006). Finally, a geochemical approach includes quantifying the ^{3}He flux in the overlying advected plume and using a ^{3}He/heat ratio measured in the vents to obtain total geothermal heat output (Jean-Baptiste et al., 1998).

Short-duration observations recorded on a single research cruise may miss the variability of hydrothermal flow, the interaction of the flow with the dynamic ocean and with living ecosys-tems, and the response of the flow to oceanographic and geophysical events. Gathering long-term time-series data using moored instrumentation is an alternate way to quantify vent fluxes and their changes over time. In this paper, we first describe evidence for diking events and associated permeability changes that may perturb the hydrothermal system. We then describe new in situ heat-flow measurements obtained from the Endeavour Segment of the Juan de Fuca Ridge, and show how techno-logical advances and the development of acoustic techniques for measuring upward velocities and volume flux have allowed capture of the effects of ocean currents on the plume. The objectives are to link buoyant hydrothermal venting to subseafloor processes and to interactions with the ambient ocean. Measurements of these plumes are then used to develop realistic models of hydrothermal heat flow in the ocean.

SEISMIC AND MAGMATIC EFFECTS ON HYDROTHERMAL SYSTEMS

By observing at the seafloor the response of mid-ocean ridge hydrothermal systems to seismic and magmatic activity, we hope to assess processes occurring at depth. Consequently, the well-recorded responses to the March 1995 seismic activity on the East Pacific Rise (EPR) near 9°50'N are of consider-able scientific interest. A continuous record of temperatures at the Bio 9 vent (Fornari et al., 1998) showed a rapid increase of approximately 7°C (Sohn et al., 1998), beginning approxi-mately four days following the seismic swarm. Figure 1a (blue line) shows the temperature record for the first year following this event, and also presents results of numerical modeling (red line) of Ramondenc et al. (2008) and Germanovich et al. (2011).

Germanovich et al. (2011) suggest that the seismic swarm may have been related to a noneruptive diking event (the filling of an existing crack with magma that can result in dike propagation and length-ening, as well as changes in surrounding crustal properties) near the west margin of the lens-shaped axial magma chamber (AMC) that increased the permeability of the discharge zone. The AMC is where magma is stored before its eruption at the sea surface, and new sets of fractures can increase the permeability, or the ability of a porous rock to transmit fluid, in the surrounding rock. A numerical model of dike propagation shows that the dike is likely to propagate subverti-cally from the lens margins, where magma replenishment would likely generate stresses and lead to the diking event, or from the edges of a discon-tinuity in the lens (Figure 1b). Using scale analysis and numerical modeling (red line in Figure 1a), mass transport in the hydrothermal system is estimated directly from the available heat flow (Ramondenc et al., 2006) and geochem-ical data (Von Damm and Lilley, 2004). Results show that an increase in vent temperature, as was observed at the seafloor only a few days after the seismic

swarm (Fornari et al., 1998; Sohn et al., 1998, 1999), does not necessarily reflect heat transported directly from the AMC or constrain the residence time of fluid in the entire discharge zone. Instead, the increase in vent temperature may have been caused by deep permeability changes associated with the same diking event. Such changes lead to a thermal perturbation in the upper 100 m of crust where high-temperature fluid mixes with cool seawater.

The analysis developed by Germanovich et al. (2011) is not restricted to the March 1995 earthquake swarm at EPR 9°50'N, but is also applicable to other locales in which coincident seismicity and thermal responses have been observed. One such example may include the events at the Main Endeavour Field (MEF) on the Juan de Fuca Ridge in June 1999, where diking was also associated with seismic (Bohnenstiehl et al., 2004), thermal (Johnson et al., 2000), and geochemical responses (Lilley et al., 2003). A non-eruptive diking event may also be associated with recently observed seismicity-hydrothermal interactions after the November 2003 swarm at the EPR near 9°50'N (Tolstoy et al., 2008).

In general, hydrothermal activity at mid-ocean ridges may be localized by diking events due to permeability enhancement near the dike margins (Delaney et al., 1986; Germanovich et al., 2000). For example, the hydrothermal sites on Endeavour Segment are located near the west margin of the seismically imaged magma lens (Bohnenstiehl et al., 2004; Van Ark et al., 2007), which suggests that the venting activity at this site may also be localized by diking triggered by lens pressurization.

Heat transfer from the AMC is the primary driver of hydrothermal systems at oceanic spreading centers. Liu and Lowell (2009) showed that quasi-stable hydrothermal heat fluxes and vent temperatures on decadal time scales require the AMC to be replenished at ~ 10^6 m^3 yr^{-1}. Such rates are consistent with estimates of magma replenishment at Axial Volcano on the Juan de Fuca Ridge following the 1998 eruption (Nooner and Chadwick, 2009) and are also consistent with the evolution of EPR lavas over the eruption cycle between 1991–1992 and 2005–2006 (Goss et al., 2010; Horne et al., 2010; Lowell et al., 2012, in this issue). AMC inflation associated with magma replenishment may lead to both eruptive and non-eruptive diking events that, in turn, may perturb the hydrothermal system and give rise to an event plume when the release of large quantities of heat results from a seismic or magmatic event at the seafloor (Lowell and Germanovich, 1995).

HYDROTHERMAL VENT FLOW MEASUREMENTS
In Situ Measurements
During four cruises to Endeavour Segment between 2008 and 2010, a significant number of new direct fluid-flow measurements were taken by the deep-submergence vehicle *Alvin* in various flow regimes, from low-temperature diffuse flow to high-temperature focused flow, on several structures within the Main Endeavour, Mothra, and High Rise hydrothermal vent fields (Germanovich et al., 2009; for a map of these vent
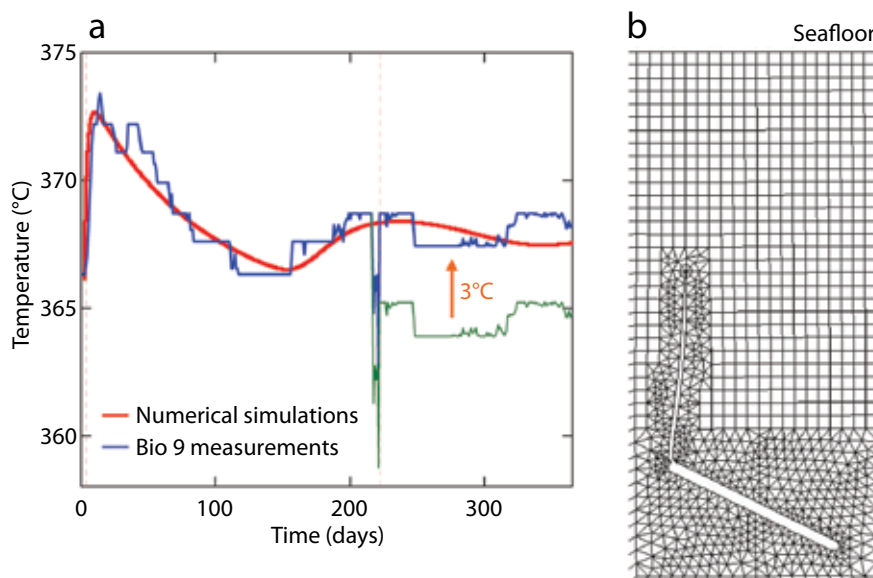
Figure 1. (a) Thermal response of the high-temperature Bio 9 vent at EPR 9°50'N following the March 1995 earthquake swarm monitored by Sohn et al. (1998) (blue curve) superimposed with the temperature response of the black smoker to a dike emplacement calculated by Germanovich et al. (2011) (red curve) based on the model developed by Ramondenc et al. (2008). The green curve after day 222 (which corresponds to the replacement of the temperature probe) represents the unchanged monitored response, while the blue line corresponds to the record translated by 3°C. Only a modest permeability increase in the vicinity of the dike leads to temperature variations at the seafloor. The shown best fit corresponds to a 40% increase with respect to the original permeability k = 1.1 x 10^{-13} m^2. (b) Finite element simulation of dike propagation from a sloping magma chamber. Based on Van Ark et al. (2007), Germanovich et al. (2011) used a pressurized inclined lens, between 2.1 and 2.5 km deep, 800 m wide, and 50 m thick. Horizontal and vertical scales are equal and the size of squared elements was 50 x 50 m. Dike propagation is from the upper tip of the magma lens. See other parameter values in Germanovich et al. (2011).

fields, see Kelley et al., 2012, in this issue). Hydrothermal fluid temperatures measured directly with *Alvin* sensors ranged from 49° to 52°C at diffuse sources and ranged up to 350°C at focused sources. Linear flow rates were measured by using relatively simple flow meters: a cup anemometer and a turbine flow meter (Figure 2). The most recently designed and tested instrument, the turbine flow meter, which uses sapphire bearings and is designed to prevent clogging by the precipitates and particles that are often encountered in hydrothermal vent discharges, was ideal in low-flow settings.

Flow velocities were estimated using the angular velocities (i.e., rotation rates) of the cup anemometer's paddle wheel or the turbine flow meter's rotor and then quantified by analysis of at least five minutes of in situ high-definition video imagery. The rotation rates of either the blades around the turbine rotor or the cups on the paddle wheel were predicted to be linearly proportional to the flow rates over a broad range of sampled flow velocities between 0.01 m s^{-1} and 2 m s^{-1}. The diffuse-flow rates displayed a range from 1 cm s^{-1} to 10 cm s^{-1}, respectively, at Dante and S&M in the MEF. However, low velocities from the focused-flow sites varied from 1 cm s^{-1} (at a "gray smoker" on Dante) up to 2 m s^{-1} (on Bambi, in the High Rise vent field) with co-registered fluid temperatures of 142°C and 350°C, respectively. Sizes of vent-chimney orifices or areal coverage of diffuse flow (based on visual observation of shimmering flow) were digitally estimated from video imagery using calibrated laser sights. Hydrothermal fluid fluxes were then calculated for each individual source based on measurement results of hydrothermal fluid flow rate, temperature, and areal extent. Typical estimates for individual vent heat flux measured at Endeavour Segment ranged from as low as 1 kW for a diffuse-flow site to as high as 10 MW on a black smoker tower.

It is difficult to determine the heat flux from an entire vent field, or even from a sulfide mound, based on scattered individual measurements. However, our broad collective heat-flow data, from the well-known active vent cluster Dante in the MEF, give an estimate of 43 MW for the total heat output. Frequent uses of direct heat-flow-measuring devices like these would certainly increase the amount of heat-flow data at mid-ocean ridges and provide baseline estimates of heat flux for input to plume models and for comparison to long-term measurements.

Acoustic Imaging (Backscatter)

Although images of black smokers shown in the lights of submerged vehicles have become iconic images of oceanography, they show only the initial meters of plume rise because of the rapid attenuation of light in water. Likewise, the actual distribution of diffuse flow surrounding black smokers is patchy on a scale of meters, so it is difficult to map optically.

Acoustics overcomes the limitations of light because sound propagates great distances in water, given an unobstructed travel path and enough energy. Acoustic methods to image, visualize, and quantify seafloor hydrothermal flow are based on the different properties of black smoker plumes and diffuse flow. The size and shape of the dynamic initial tens of meters of a buoyantly rising black smoker plume is imaged using backscatter of an acoustic pulse from suspended metallic mineral particles and turbulent temperature fluctuations (Figure 3). The scattering depends on the physical properties of the small particles (Palmer and Rona, 2005) and the characteristics of turbulent sound speed and density fluctuations related primarily to temperature (Ostashev, 1994; Ross, 2003).

Determining plume fluxes also requires measurement of flow rates. Doppler algorithms are used to measure

Figure 2. Positive displacement flow meters are shown in situ at the Dante sites (Main Endeavour Field, Juan de Fuca Ridge) while spinning and measuring linear flow velocity to determine the amount of fluid that is being displaced between the (a) cup anemometer's paddle wheels or (b) turbine flow meter's blades. The turbine flow meter incorporates a titanium rotor assembly housed within a stainless steel cylindrical body and supported by sapphire bearings.

flow velocity in cross section and mean vertical velocity at different altitudes in a plume (Jackson et al., 2003). As the sonar can only measure velocity along the line-of-sight direction, a simple geometric correction is made to estimate the plume velocity's vertical component, compensating for the ambient current. Integration of velocity produces volume flux through the various cross sections.

The acoustic scintillation thermography (AST) method was developed to detect and map diffuse flow in seafloor hydrothermal fields (Rona et al., 1997; Rona and Jones, 2009). AST exploits the same principle as the human eye for detecting warm water—the scintillation of an acoustical or optical wave as it passes through a turbulent flow field and scatters off the underlying seafloor. Index of refraction changes from temporal fluctuations, caused by turbulent mixing of the warm water, distorts and decorrelates successive acoustic transmissions. The diffuse-flow area is inferred from the spatial distribution of such distortions.

The output of multiple plumes and entrained diffuse and flange flow tends to merge above a seafloor hydrothermal field, so acoustic methods open the possibility of obtaining both integrated volume flux and heat flux for a field. Initial estimates of partitioning of heat flux from black smokers and surrounding diffuse flow were made using direct measurements of temperature and flow rates. Direct measurements in the small Ashes vent field (~ 50 m in diameter with five black smokers and intervening diffuse flow) at Axial Volcano indicate that the heat from diffuse flow (15–75 MW) is an order of magnitude greater than that from black smokers (4.4 ± 2 MW; Rona and Trivett, 1992). Direct measurements of diffuse and focused flow from a sulfide

body in the MEF indicate diffuse flow exceeding focused flow by a factor of five (Schultz et al., 1992). Typical heat flux from a flange is relatively small (~ 1 MW; Woods and Delaney, 1992), but output from multiple flanges may be cumulatively significant as they rise and become entrained in plumes. Preliminary values using a combination of acoustic measurement of diffuse-flow area and direct measurement of smokers' temperature and flow rates, and diffuse flow from a sulfide edifice in the Grotto vent cluster in the MEF, suggest an

even larger ratio (smokers ~ 42 MW; surrounding diffuse flow > 990 MW; Rona et al., 2010).

Acoustical Scintillation (Forward Scatter)

The application of acoustical scintillation to ocean measurement has its origin in the interpretation of electromagnetic or acoustic signal modulations from atmospheric refractive index irregularities convected across the path between a transmitter and a receiver separately located (Tatarskii, 1971). For
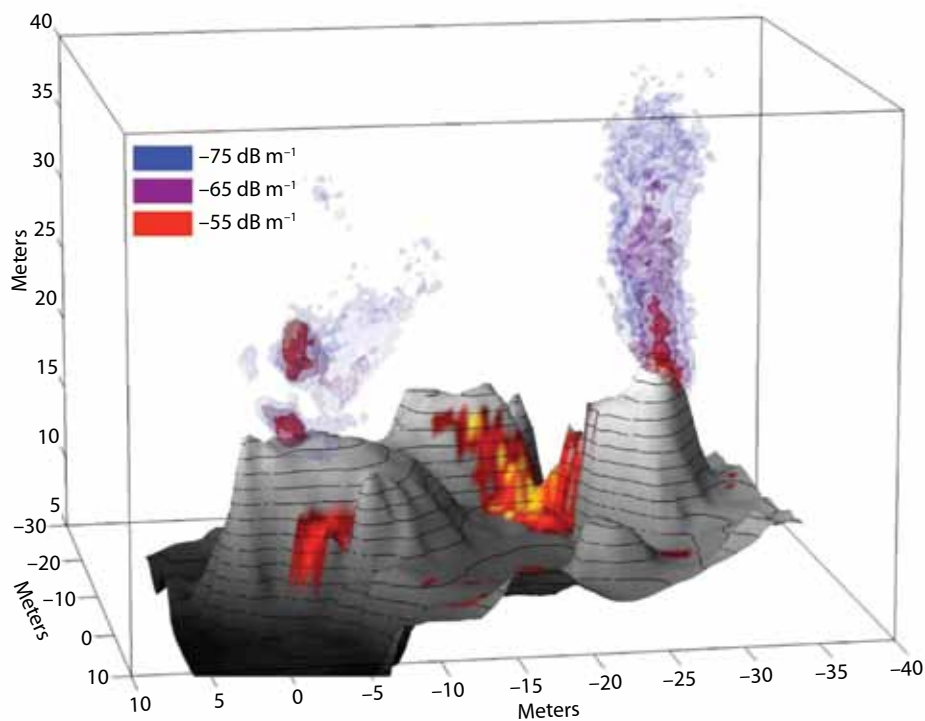
Figure 3. Cabled Observatory Vent Imaging Sonar (COVIS) acoustic image made at 0800 UT on October 1, 2010, looking south at black smoker plumes and areas of diffuse flow draped over bathymetry of the Grotto vent cluster in Main Endeavour Field, Juan de Fuca Ridge (horizontal and vertical axes scaled in meters; COVIS at position 0, 0). The COVIS instrument is connected to the NEPTUNE Canada Cabled Observatory. The image was made near slack tide when tidal currents were minimal and the plumes were nearly vertical. The large plume is from the north tower edifice at the northwestern end, and the smaller plumes are from the northeastern end, of Grotto where in situ experiments of other investigators are located. The legend specifies isosurfaces of plume volume scattering strengths (decibels per meter) related to particle content and temperature discontinuities. The plumes decrease in acoustic backscatter with rise height (meters) above vents, as they mix with surrounding seawater. Areas of diffuse flow mapped by the acoustic scintillation thermography method are draped over the bathymetry with the most intense flow (highest decorrelation in backscatter) shown in yellow decreasing outward to red (color legend not shown; Rona and Jones, 2009). *Bathymetry courtesy D. Clague, MBARI; modified from Rona and Light (2011). Image courtesy of C.D. Jones, Applied Physics Laboratory, University of Washington*

hydrothermal plumes, sound-speed variations from temperature forward scatter the spherically spreading acoustical wave fronts as they travel through the plume (see Figure 4a), resulting in amplitude fluctuations at the receivers. These fluctuations are referred to as scintillations and are analogous to the "twinkling" of stars as a result of the turbulent atmosphere.

The remotely operated vehicle (ROV) *Jason 2* deployed a self-contained battery-operated mobile system, consisting of transmitter and receiver moorings (see Figure 4a), on either side

of the Dante mound for six weeks of data collection. Figure 4b shows the spectrum for the log-amplitude fluctuations, modified for hydrothermal vents having a path-dependent Gaussian distribution for temperature variations (Xu and Di Iorio, 2011), with a comparison to the measured spectrum. The range of turbulent scales presented by the spectrum is from 14 m to 3 cm. Such a range is based on the assumption that the largest turbulence within the plume is of the order of the plume's diameter (~ 14 m at 20 m above the orifice, according to

the acoustic image in Figure 4a), and the smallest scale that can be resolved by the acoustic instrument that contributes to the sound speed fluctuations is ~ 3 cm. The most sensitive scale at the peak of the spectrum is the Fresnel scale (0.7 m is the minimum scale that can focus the acoustic energy to the receivers—anything smaller will be masked by diffraction effects). According to Figure 4b, a –5/3 slope exists, which suggests the validity of applying the universal power spectrum hypothesized by Kolmogorov for isotropic and
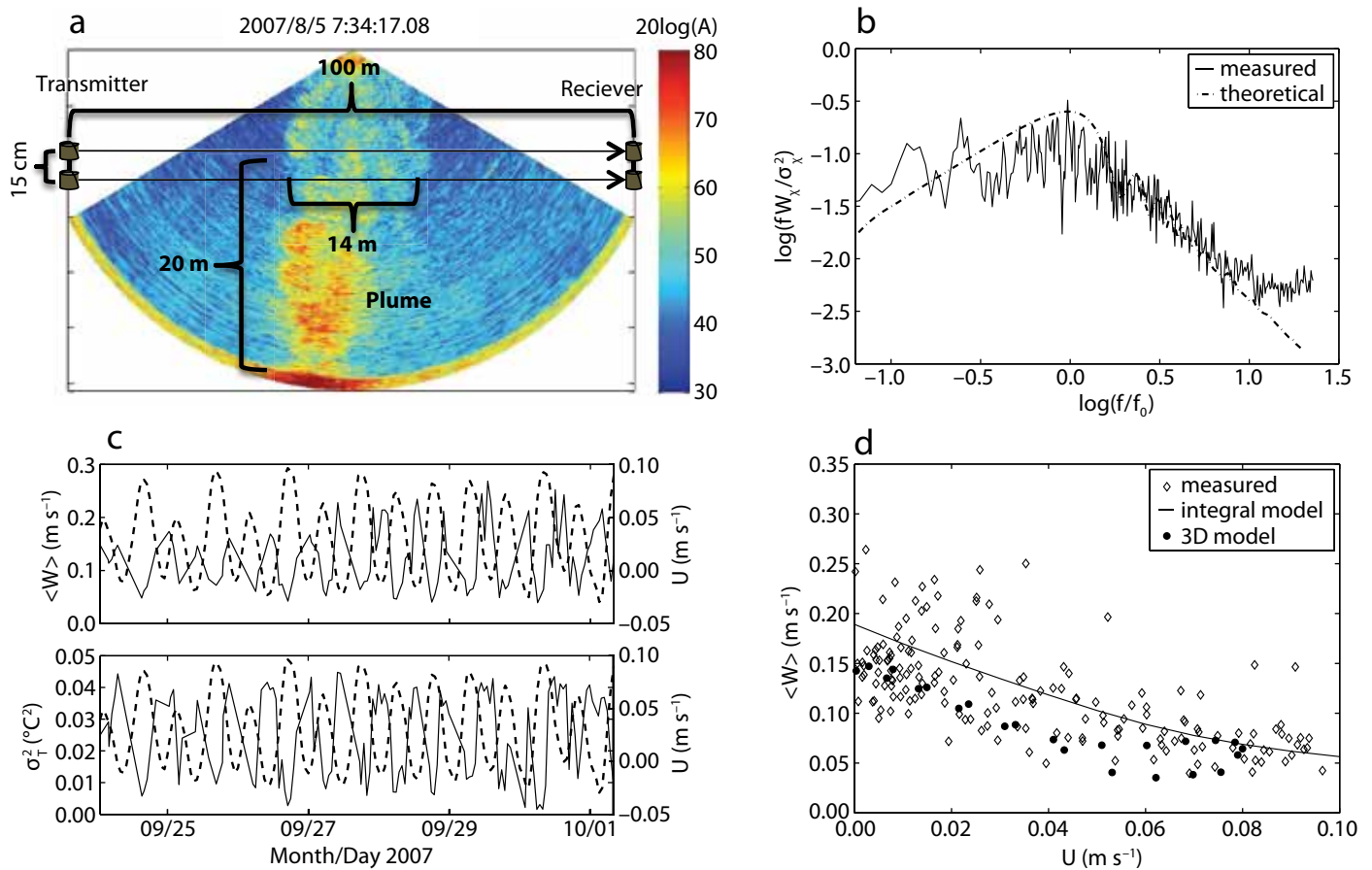
Figure 4. (a) A downward-looking acoustic backscatter image taken from the remotely operated vehicle *Jason 2* while hovering at 30 m above the Dante hydrothermal vent structure. Diagram shows the placement of the acoustic scintillation transmitter and receiver arrays at 20 m above and the acoustic propagation through the buoyant plume. (b) A comparison of the measured log-amplitude power spectrum with the theoretical curve (dashed line), assuming weak scattering and a Kolmogorov turbulence model for the temperature fluctuations. (c) The path averaged vertical velocity and temperature variance (solid curves) plotted with the extrapolated horizontal currents aligned along the acoustic propagation direction (dashed lines). (d) A comparison among measured (diamonds), integral model (solid line), and the three-dimensional (3D) model (solid dots) of the radially averaged vertical velocity at 20 m above as a function of the background horizontal cross flow. Both models assume a total heat flux of 25 MW, and the integral model assumes entrainment coefficients $\alpha = 0.1$ and $\beta = 0.6$, and drag coefficient $C_D = 1.7$. Note that the 3D model shows hysteresis in the vertical velocity (i.e., the vertical velocity for increasing horizontal flows is lower than for decreasing flows).

homogenous temperature fluctuations (Tatarskii, 1971; Xu and Di Iorio 2011).

Fine-structure variability in the medium transported by the buoyancy-driven plume will create a space-time scintillation pattern over vertically spaced receivers. Detection of this pattern's motion is the essential concept exploited in acoustical scintillation. Using space-time coherence methods (Farmer et al., 1987) and calculating the time-lagged cross covariance of the log-amplitude fluctuations (from acoustic paths separated by 15 cm) yields path-averaged vertical flow. Figure 4c shows the vertical velocity and the temperature variance (derived from the log-amplitude variance) of the Dante hydrothermal plume (measured at 20 m above the orifice) over eight days, with average values of 0.14 m s^{-1} and 0.03 ($°C$)^2, respectively. Tidal oscillations can be observed in both measurements. Spectral analysis for a six-week time series shows that the oscillations are forced at two dominant frequencies: the M2 tidal constituent and the four-day oscillation observed by Cannon and Thomson (1996) in the current meter measurements within the Endeavour Segment axial valley.

According to Allen and Thomson (1993) and Thomson et al. (2003), the tidal oscillations within Endeavour's axial valley are attenuated, and the M2 oscillation is the most dominant frequency. The mean residual flow within the axial valley is near steady and convergent. At the southern and central parts of the axial valley, the mean flow is predominantly northward and strongest (5 cm s^{-1}), while at the northern part of the valley, the mean flow becomes southward and weakest (1 cm s^{-1}). Entrainment into the hydrothermal plumes is thought to induce the convergent mean flow within

the axial valley (Thomson et al., 2003, 2005). The northward mean flow extends to the central valley due to the shallow topographic saddle at the axial valley's northern end and more intensive hydro-thermal activity within the southern and central valley.

Tidal currents within the axial valley during the 2007 acoustic scintillation deployment can be extrapolated from 2001 current meter data (obtained from Rick Thomson, Institute of Ocean Sciences, Fisheries and Oceans Canada) using the T-Tide harmonic analysis program (Pawlowicz et al., 2002), as no tidal flow observation was available during the time of this measurement. The horizontal flow was estimated by adding a northward mean residual flow that is characteristic in the MEF. Figure 4c shows that the estimated horizontal flow, aligned along the acoustic propagation direction, reaches a maximum during flooding tide and is small during the ebbing tide. A significant negative correlation between the vertical velocity/temperature variance and the horizontal flow is observed (r ~ −0.55/−0.53).

ANALYTIC AND NUMERICAL MODELS OF HOT-SOURCE WATER-COLUMN HYDROTHERMAL PLUMES

Factors that affect the distribution of hot-source hydrothermal plumes in the water column include local ocean stratification, latitude of the site, ambient ocean circulation, and the nature of the source. The last factor involves consideration of source size and configuration, thermal output, source salinity anomaly, source duration, and possibly small-scale local topography. Needless to say, the number of permutations of these factors ensures that only a small fraction of the potential

outcomes have yet been modeled.

In plume dynamics, ambient stratification is important in determining how high into the water column a plume will rise because upward motion will essentially stop at a height where the density of the plume, diluted while rising, matches the density of the surrounding ocean. The latitude of the site can be important because Earth's rotation affects the horizontal flow generated by entrainment into the rising buoyant plume and deflections around the plume itself. Flow in the ambient ocean that receives the hydrothermal discharge is likely to be spatially and temporally complicated, but existing models of hydrothermal plumes have simplified flow in both regards by assuming the spatial homogeneity of the background motion, and either no flow, steady cross flow, idealized nonsteady flow, or a flow time series taken from ocean observations. Source characterization is perhaps the most difficult of the factors to quantify. Source fluxes, which are the product of source area, discharge velocity, and temperature or salinity anomalies with respect to the background ocean, in many cases have not been or cannot be measured (previous sections discuss the available measurements for the MEF). In a number of cases, geometrically small sources are seemingly randomly distributed over areas of a few tens of meters squared (i.e., a vent field), and the plume well above the individual discharges is a composite of all sources. When source flux cannot be directly measured, it must be estimated from water-column measurements of the plume.

Integral Models
The analytic mathematical Morton-Taylor-Turner (MTT) model (Morton et al., 1956) was the earliest used to

describe hydrothermal plume ascent (see examples of applications in Speer and Rona, 1989; Rudnicki and Elderfield, 1992; McDuff, 1995). MTT assumes a plume that is radially symmetric about a vertical axis and entrainment into the plume stem that is directly proportional to the upward stem velocity. That model usefully provides a first estimate of the height where the plume might achieve neutral buoyancy and yields vertical profiles of plume properties as a function of elevation within the plume stem. However, it cannot address properties of the plume at the level of neutral buoyancy, and MTT also presupposes a quiescent environment into which the plume rises. The MTT model falls into the category of "integral models" because, in effect, its radial dependencies are integrated out after assuming that the constituent variables of the model can be represented as products of plume axis functions and a common function for radial dependence. In integral models, the function separability assumption and a subsequent radial integration changes the equation set from one of partial to ordinary differential equations, which are easier to solve numerically.

Because ocean sites with negligible cross flow are few and far between, Fan (1967) modified the MTT model to include horizontal cross flows and a drag force imposed by the horizontal flow. According to laboratory experiments carried out by Fan (1967), cross flow enhances entrainment. Hoult and Weil (1972), Webster and Thomson (2002), and Devenish et al. (2010) then parameterized the entrainment velocity as a linear addition of the relative velocity components along the plume axis (with entrainment coefficient α) and normal to the plume boundary (with entrainment coefficient β) when cross flows

exist. In this context, the ambient cross flow "blows" water into the plume and the plume itself "breathes" water in. Thus, when the horizontal cross flow is weak, less ambient ocean water will be entrained into the plume. In such a case, the plume will be faster and hotter, causing temperature fluctuations to increase. When the horizontal flow is strong, more ambient ocean water is entrained into the plume, causing it to bend. In such a case, the plume will be slower and cooler, with reduced temperature fluctuations.

The parameter values for the integral model representation of the plume from Dante were set to a total heat flux of 25 MW and correspond to a cumulative areal radius of 0.14 m (area = 0.06 m^2), an initial velocity of 0.3 m s^{-1}, a temperature anomaly of 324°C, and a salinity deficit of 5.3 as documented by Butterfield et al. (1994). The model is forced with a horizontal cross flow varying from 0 to 0.1 m s^{-1}. The plume's radial-averaged vertical velocity is computed at z = 20 m above the orifice and is plotted as a function of the horizontal cross flow in Figure 4d. The curve that gives the best fit to our measurements represents entrainment coefficients α = 0.1 and β = 0.6, and a drag coefficient (C_D = 1.7) that is in the range proposed by Fan (1967). Measurement of the acoustically derived vertical velocity, which is a spatial average through the plume, is also plotted against the extrapolated horizontal currents. The model supports the idea that entrainment of the ambient seawater into the plume is enhanced under a strong horizontal cross flow, which makes the plume cooler and slower than when the horizontal flow is weak, and provides a means to quantify the source conditions.

Three-Dimensional Numerical Modeling

A second category of models for hydrothermal plumes embodies a full three-dimensional, nonlinear, nonhydrostatic partial differential equation set for mass, momentum, and property (heat and salt) conservation, along with auxiliary equations for turbulence. One of the first applications of this type of model was in the description of the initial hours of a megaplume formation (Lavelle and Baker, 1994; Lavelle, 1995). Speer (1997) used such a model to examine the possibility of a megaplume crossing the shallow upper-ocean thermocline and expressing itself at the sea surface. In all such cases, the length scales of the megaplumes (order tens of kilometers) make Earth's rotation an important factor. As the megaplume rises, fluid rushes radially inward into the ephemeral megaplume stem, while the opposite occurs aloft. As the fluid nears the level of neutral buoyancy, the fluid flows radially outward, and Earth's rotation causes the megaplume to rotate anticyclonically (clockwise in the Northern Hemisphere and counter clockwise in the Southern Hemisphere).

A hydrodynamical-transport-turbulence model of the same type has been used in the case of steady ambient cross flows (Lavelle, 1997). Cross flows complicate the calculations because the domain must be effectively open to outward heat transport. The three-dimensional model results for an aggregated (vent-field) source show the plume bifurcating downstream, a feature often observed in atmospheric plumes. The model results also allow calculation of rise height as a function of cross flow, and entrainment as a function of height. In these models, no explicit assumption needs to be made about the nature of entrainment. Lavelle and Wetzler (1999)

also used the model to study the entrainment of diffuse sources and background materials into a strongly rising plume.

The extension of the same model to the case of time variable cross flow allows comparisons to be made with time-series measurements across the buoyant plume stem at the Dante mound (Figure 4). That location is known to have a relatively strong M2 tidal current and a northward steady flow of comparable magnitude. The model was also configured with a source heat flux of 25 MW, which corresponds to an aggregate discharge area 6 m x 6 m, a negative salinity anomaly at the source of 5, and a cross-stream tidal velocity represented by $u = 0.04 + 0.04\sin(2\pi t/T_{M2})$, where t is time and $T_{M2} = 12.42$ hr, the principal

lunar tidal period. A sequence of plume cross sections (horizontal at 20 m above the Dante mound and vertical in Figure 5) shows potential temperature anomalies over a cross-stream cycle. The plume bends to be nearly horizontal in the strongest flows, and rises approximately 200 m above the vent field near slack flow. At maximum horizontal flow, enhanced entrainment occurs on the upstream side of the stem and backflow occurs on the downstream side. Figure 4d shows the three-dimensional model results for the radially averaged vertical velocity versus the background horizontal flow for comparisons with measurements and the integral model. The three-dimensional model gives similar results and also includes new

information on hysteresis (i.e., vertical velocity is less for increasing horizontal flows than decreasing horizontal flows).

CONCLUSIONS

With the development and installation of cabled observatories like NEPTUNE Canada (http://www.neptunecanada.ca) at Endeavour Segment and the Regional Cabled Component (http://www.ooi. washington.edu/rsn) at Axial Volcano, it will be possible to start linking hydrothermal discharges to seismic and magmatic events and to ocean processes. Long-term time series of plume properties (shape, vertical velocity, temperature fluctuations, volume flux) and diffuse flow (aerial extent) obtained by acoustic methods, together with in situ measurements (seismicity, temperature, video imagery, currents, stratification), will make it possible to understand the spatial and temporal variations of heat flow. These measurements can then be used to refine plume models to yield insights into entrainment, plume bending, and rise height, and to infer mound heat flux.
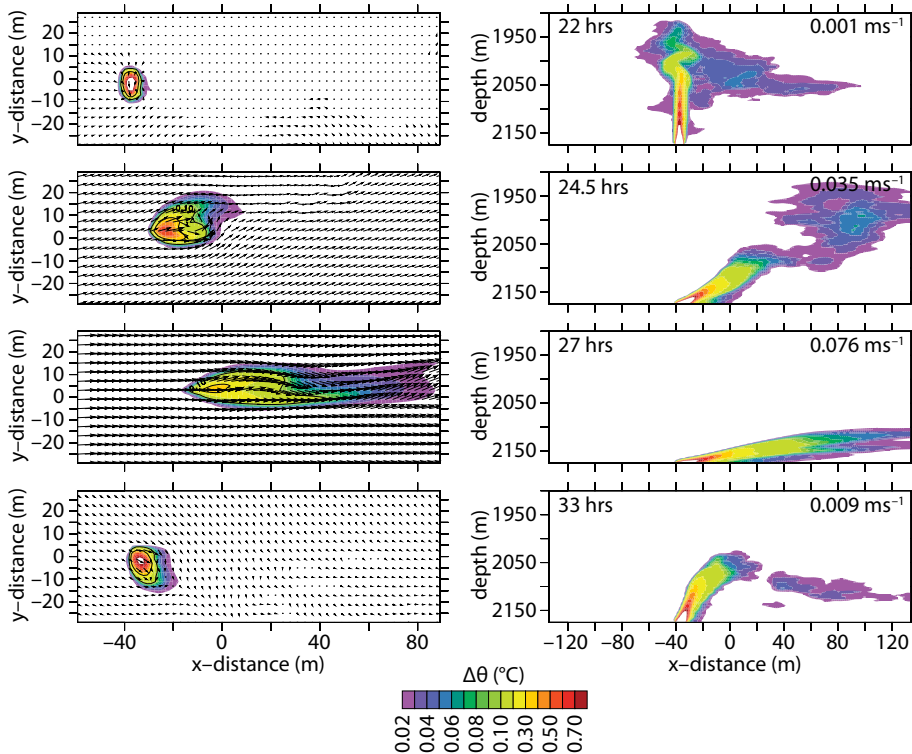
Figure 5. Horizontal (at 20 m above with horizontal flows, left) and vertical (right) cross sections of potential temperature anomaly ($\Delta\theta$) for a model vent field discharging into a time-dependent tidal flow. Time and flow speed are shown in the panels to the right. Cross flow is $u = 0.04(1 + \sin \omega t)$, $v = 0.01\cos \omega t$ in units of m s^{-1}, with $\omega = 2\pi/(12.42$ hrs). Source area is 36 m^2 with an output of 25 MW of heat, an upward velocity of 0.1 m s^{-1} at the seafloor, and fluids having a negative salinity anomaly of 5.3. Because the plume wanders slightly back and forth across the mean downstream direction, values on each of these downstream-depth (x-y) transects represent the normal projection of $\Delta\theta$ maxima onto that plane.

REFERENCES

Allen, S.E., and R.E. Thomson. 1993. Bottom-trapped subinertial motions over midocean ridges in a stratified rotating fluid. *Journal of Physical Oceanography* 23:566–581, http://dx.doi.org/10.1175/1520-0485(1993)023<0566:BTSMOM>2.0.CO;2.

Baker, E.T., and G.J. Massoth. 1987. Characteristics of hydrothermal plumes from two vent fields on the Juan de Fuca Ridge, Northeast Pacific Ocean. *Earth and Planetary Science Letters* 85:59–73, http://dx.doi.org/10.1016/0012-821X(87)90021-5.

Bemis, K., R.P. Lowell, and A. Farough. 2012. Diffuse flow on and around hydrothermal vents at mid-ocean ridges. *Oceanography* 25(1):182–191, http://dx.doi.org/10.5670/oceanog.2012.16.

Bemis, K.G., R.P. von Herzen, and M.J. Mottl. 1993. Geothermal heat flux from hydrothermal plumes on the Juan de Fuca Ridge. *Journal of Geophysical Research* 98:6,351–6,369, http://dx.doi.org/10.1029/92JB02273.

Bohnenstiehl, D.R., R.P. Dziak, M. Tolstoy, C.G. Fox, and M. Fowler. 2004. Temporal and spatial history of the 1999–2000 Endeavour Segment seismic series, Juan de Fuca Ridge. *Geochemistry Geophysics Geosystems* 5, Q09003, http://dx.doi.org/10.1029/2004GC000735.

Butterfield, D.A., R.E. McDuff, M.J. Mottl, M.D. Lilley, J.E. Lupton, and G.J. Massoth. 1994. Gradients in the composition of hydrothermal fluids from the Endeavour Segment vent field: Phase separation and brine loss. *Journal of Geophysical Research* 99:9,561–9,583, http://dx.doi.org/10.1029/93JB03132.

Cannon, G.A., and R.E. Thomson. 1996. Characteristic 4-day oscillations trapped by the Juan de Fuca Ridge. *Geophysical Research Letters* 23:1,613–1,616, http://dx.doi.org/10.1029/96GL01370.

Delaney, P.T., D.D. Pollard, J.I. Ziony, and E.H. Mckee. 1986. Field relations between dikes and joints: Emplacement processes and paleostress analysis. *Journal of Geophysical Research* 91(B5):4,920–4,938, http://dx.doi.org/10.1029/JB091iB05p04920.

Devenish, B.J., G. Rooney, H. Webster, and D. Thomson. 2010. The entrainment rate for buoyant plumes in a crossflow. *Boundary-Layer Meteorology* 134:411–439, http://dx.doi.org/10.1007/s10546-009-9464-5.

Fan, L.-N. 1967. *Turbulent Buoyant Jets into Stratified or Flowing Ambient Fluids.* Technical Report No. KH-R-15, California Institute of Technology, Pasadena, CA.

Farmer, D.M., S.F. Clifford, and J.A. Verrall. 1987. Scintillation structure of a turbulent tidal flow. *Journal of Geophysical Research* 92:5,369–5,382, http://dx.doi.org/10.1029/JC092iC05p05369.

Fornari, D.J., T. Shank, K.L. Von Damm, T.K.P. Gregg, M. Lilley, G. Levai, A. Bray, R.M. Haymon, M.R. Perfit, and R. Lutz. 1998. Time-series temperature measurements at high-temperature hydrothermal vents, East Pacific Rise 9°49'–51'N: Evidence for monitoring a crustal cracking event. *Earth and Planetary Science Letters* 160:419–431, http://dx.doi.org/10.1016/S0012-821X(98)00101-0.

Germanovich, L.N., D. Di Iorio, G. Genc, R.S. Hurt, R.P. Lowell, J.F. Holden, D.A. Butterfield, and E.J. Olson. 2009. Direct measurements of hydrothermal heat output at Juan de Fuca Ridge. *Eos, Transactions, American Geophysical Union* 90(52): Fall Meeting Abstract OS13A–1179.

Germanovich, L.N., R.P. Lowell, and D.K. Astakhov. 2000. Stress dependent permeability and the formation of seafloor event plumes. *Journal of Geophysical Research* 105(B4):8,341–8,354, http://dx.doi.org/10.1029/1999JB900431.

Germanovich, L.N., R.P. Lowell, and P. Ramondenc. 2011. Magmatic origin of hydrothermal response to earthquake swarms: Constraints from heat flow and geochemical data. *Journal of Geophysical Research* 116, B05103, http://dx.doi.org/10.1029/2009JB006588.

Ginster, U., and M.J. Mottl. 1994. Heat flux from black smokers on the Endeavour and Cleft segments, Juan de Fuca Ridge. *Journal of Geophysical Research* 99:4,937–4,950, http://dx.doi.org/10.1029/93JB02800.

Goss, A.R., M.E. Perfit, W.I. Ridley, K.H. Rubin, G.D. Kamenov, S.A. Soule, A. Fundis, and D.J. Fornari. 2010. Geochemistry of lavas from the 2005–2006 eruption at the East Pacific Rise, 9°46'N–9°56'N: Implications for ridge crest plumbing and decadal changes in magma chamber compositions. *Geochemistry Geophysics Geosystems* 11, Q05T09, http://dx.doi.org/10.1029/2009GC002977.

Horne, R., L. Hebert, L. Liu, and R. Lowell. 2010. Fractional crystallization and replenishment of the magma chamber at the East Pacific Rise 9°50'N. *Eos, Transactions, American Geophysical Union* 91(52): Fall Meeting Abstract OS21C-1507.

Hoult, D.P., and J.C. Weil. 1972. Turbulent plume in a laminar cross flow. *Atmospheric Environment* 6:513–531, http://dx.doi.org/10.1016/0004-6981(72)90069-8.

Jackson, D.R., C.D. Jones, P.A. Rona, and K.G. Bemis. 2003. A method for Doppler acoustic measurement of black smoker flow fields. *Geochemistry Geophysics Geosystems* 4(11), 1095, http://dx.doi.org/10.1029/2003GC000509.

Jean-Baptiste, P., H. Bougault, A. Vangriesheim, J.L. Charlou, J. Radford-Knoery, Y. Fouquet, D. Needham, and C. German. 1998. Mantle ^{3}He in hydrothermal vents and plume of the Lucky Strike site (MAR 37°17'N) and associated geothermal heat flux. *Earth and Planetary Science Letters* 157:69–77, http://dx.doi.org/10.1016/S0012-821X(98)00022-3.

Johnson, H.P., M. Hutnak, R.P. Dziak, C.G. Fox, I. Urcuyo, J.P. Cowen, J. Nabelek, and C. Fisher. 2000. Earthquake-induced changes in a hydrothermal system on the Juan de Fuca mid-ocean ridge. *Nature* 407:174–177, http://dx.doi.org/10.1038/35025040.

Kelley, D.S., S.M. Carbotte, D.W. Caress, D.A. Clague, J.R. Delaney, J.B. Gill, H. Hadaway, J.F. Holden, E.E.E. Hooft, J.P. Kellogg, and others. 2012. Endeavour Segment of the Juan de Fuca Ridge: One of the most remarkable places on Earth. *Oceanography* 25(1):44–61, http://dx.doi.org/10.5670/oceanog.2012.03.

Lavelle, J.W. 1995. The initial rise of a hydrothermal plume from a line segment source: Results from a three-dimensional numerical model. *Geophysical Research Letters* 22(2):159–162, http://dx.doi.org/10.1029/94GL01463.

Lavelle, J.W. 1997. Buoyancy-driven plumes in rotating, stratified cross flows: Plume dependence on rotation, turbulent mixing, and cross-flow strength. *Journal of Geophysical Research* 102(C2):3,405–3,420, http://dx.doi.org/10.1029/96JC03601.

Lavelle, J.W., and E.T. Baker. 1994. A numerical study of local convection in the benthic ocean induced by episodic hydrothermal discharges. *Journal of Geophysical Research* 99(C8):16,065–16,080, http://dx.doi.org/10.1029/94JC01203.

Lavelle, J.W., and M.A. Wetzler. 1999. Diffuse venting and background contributions to chemical anomalies in a neutrally buoyant ocean hydrothermal plume. *Journal of Geophysical Research* 104(C2):3,201–3,209, http://dx.doi.org/10.1029/1998JC900063.

Lilley, M.D., D.A. Butterfield, J.E. Lupton, and E.J. Olson. 2003. Magmatic events can produce rapid changes in hydrothermal vent chemistry. *Nature* 422:878–881.

Liu, L., and R.P. Lowell. 2009. Models of hydrothermal heat output from a convecting, crystallizing, replenished magma chamber beneath an oceanic spreading center. *Journal of Geophysical Research* 114, B02102, http://dx.doi.org/10.1029/2008JB005846.

Lowell, R.P., A. Farough, L.N. Germanovich, L.B. Hebert, and R. Horne. 2012. A vent-field-scale model of the East Pacific Rise 9°50'N magma-hydrothermal system. *Oceanography* 25(1):158–167, http://dx.doi.org/10.5670/oceanog.2012.13.

Lowell, R.P., and L.N. Germanovich. 1995. Dike injection and the formation of megaplumes at ocean ridges. *Science* 267:1,804–1,807, http://dx.doi.org/10.1126/science.267.5205.1804.

McDuff, R.E. 1995. Physical dynamics of deep-sea hydrothermal plumes. Pp. 357–368 in *Seafloor Hydrothermal Systems: Physical, Chemical, Biological, and Geological Interactions.* S.E. Humphris, R.A. Zierenberg, L.S. Mullineaux, and R.E. Thomson, eds, Geophysical Monograph Series, vol. 91, American Geophysical Union, Washington, DC.

Morton, B., G. Taylor, and J. Turner. 1956. Turbulent gravitational convection from maintained and instantaneous sources. *Proceedings of the Royal Society of London A* 234:1–23, http://dx.doi.org/10.1098/rspa.1956.0011.

Nooner, S.L., and W.W. Chadwick Jr. 2009. Volcanic inflation measured in the caldera of Axial Seamount: Implications for magma supply and future eruptions. *Geochemistry Geophysics Geosystems* 10, Q02002, http://dx.doi.org/10.1029/2008GC002315.

Ostashev, V.E. 1994. Sound propagation and scattering in media with random inhomogeneities of sound speed, density and medium velocity. *Waves in Random Media* 4:403–428, http://dx.doi.org/10.1088/0959-7174/4/4/001.

Palmer, D.R., and P.A. Rona. 2005. Acoustical imaging of deep ocean hydrothermal flows. Pp. 551–563 in *Sounds in the Sea: From Ocean Acoustics to Acoustical Oceanography*. H. Medwin, ed., Cambridge University Press.

Pawlowicz, R., B. Beardsley, and S. Lentz. 2002. Classical tidal harmonic analysis including error estimates in MATLAB using T-TIDE. *Computers &Geosciences* 28:929–937, http://dx.doi.org/10.1016/S0098-3004(02)00013-4.

Ramondenc, P., L.N. Germanovich, and R.P. Lowell. 2008. Modeling the hydrothermal response to earthquakes with application to the 1995 event at 9°50'N, East Pacific Rise. Pp. 97–122 in *Magma to Microbe: Modeling Hydrothermal Processes at Oceanic Spreading Centers*. R.P. Lowell, J.S. Seewald, A. Metaxas, and M.R. Perfit, eds, Geophysical Monograph Series, vol. 178, American Geophysical Union, Washington, DC.

Ramondenc, P., L.N. Germanovich, K.L. Von Damm, and R.P. Lowell. 2006. The first measurements of hydrothermal heat output at 9°50'N, East Pacific Rise. *Earth and Planetary Science Letters* 245:487–497, http://dx.doi.org/10.1016/j.epsl.2006.03.023.

Rona, P.A., K.G. Bemis, C.D. Jones, D.R. Jackson, K. Mitsuzawa, and D.R. Palmer. 2010. Partitioning between plume and diffuse flow at the Grotto Vent cluster, Main Endeavour Vent Field, Juan de Fuca Ridge: Past and present. *Eos, Transactions, American Geophysical Union* 91(52):Fall Meeting Abstract OA21C-1519.

Rona, P.A., D.R. Jackson, T. Wen, C. Jones, K. Mitsuzawa, K.G. Bemis, and J.G. Dworski. 1997. Acoustic mapping of diffuse flow at a seafloor hydrothermal site: Monolith Vent, Juan de Fuca Ridge. *Geophysical Research Letters* 24:2,351–2,354, http://dx.doi.org/10.1029/97GL02504.

Rona, P.A., and C.D. Jones. 2009. Acoustic scintillation thermography. Pp. 71–74 in *Encyclopedia of Ocean Sciences*, 2nd ed. Elsevier Ltd., http://dx.doi.org/10.1016/B978-012374473-9.00735-9.

Rona, P., and R. Light. 2011. Sonar images hydrothermal vents in seafloor observatory. *Eos, Transactions, American Geophysical Union* 92(20):169, http://dx.doi.org/10.1029/2011EO200002.

Rona, P.A., and D.A. Trivett. 1992. Discrete and diffuse heat transfer at ASHES vent field, Axial Volcano, Juan de Fuca Ridge. *Earth and Planetary Science Letters* 109:57–71, http://dx.doi.org/10.1016/0012-821X(92)90074-6.

Rosenberg, N.D., J.E. Lupton, D. Kadko, R. Collier, M.D. Lilley, and H. Pak. 1988. Estimation of heat and chemical fluxes from a seafloor hydrothermal vent field using radon measurements. *Nature* 334:604–607, http://dx.doi.org/10.1038/334604a0.

Ross, T. 2003. *Sound Scattering from Oceanic Turbulence*. PhD Thesis, University of Victoria, Victoria, BC.

Rudnicki, M.D., and H. Elderfield. 1992. Theory applied to the Mid-Atlantic Ridge hydrothermal plumes: The finite-difference approach. *Journal of Volcanology and Geothermal Research* 50:161–172, http://dx.doi.org/10.1016/0377-0273(92)90043-D.

Schultz, A., J.R. Delaney, and R.E. McDuff. 1992. On the partitioning of heat flux between diffuse and point source seafloor venting. *Journal of Geophysical Research* 97(B9):12,299–12,314, http://dx.doi.org/10.1029/92JB00889.

Sohn, R.A., D.J. Fornari, K.L. Von Damm, J.A. Hildebrand, and S.C. Webb. 1998. Seismic and hydrothermal evidence for a cracking event on the East Pacific Rise crest at 9°50'N. *Nature* 396:159–161, http://dx.doi.org/10.1038/24146.

Sohn, R.A., J.A. Hildebrand, and S.C. Webb. 1999. A microearthquake survey of the high-temperature vent fields on the volcanically active East Pacific Rise (9°50'N). *Journal of Geophysical Research* 104(B11):25,367–25,377, http://dx.doi.org/10.1029/1999JB900263.

Speer, K.G. 1997. Thermocline penetration by buoyant plumes. *Philosophical Transactions of the Royal Society of London A* 355:443–457, http://dx.doi.org/10.1098/rsta.1997.0016

Speer, K.G., and P.A. Rona. 1989. A model of an Atlantic and Pacific hydrothermal plume. *Journal of Geophysical Research* 94(C5):6,213–6,220, http://dx.doi.org/10.1029/JC094iC05p06213.

Stahr, F.R., R.E. McDuff, D.R. Yoerger, A.M. Bradley, and K. Nakamura. 2000. Heat flux measurements at the Main Endeavour vent field, Juan de Fuca Ridge. *Eos, Transactions, American Geophysical Union* 81(48):Abstract OS521–03.

Tatarskii, V.I. 1971. *The Effects of the Turbulent Atmosphere on Wave Propagation*. Israel Program for Scientific Translation Ltd., Jerusalem, reproduced by NTIS, US Department of Commerce, Springfield, VA, Technical Translation 68-50464, 472 pp.

Thomson, R., E.E. Delaney, R.E. McDuff, D.R. Janecky, and J.S. McClain. 1992. Physical characteristics of the Endeavour Ridge hydrothermal plume during July 1988. *Earth and Planetary Science Letters* 111:141–154, http://dx.doi.org/10.1016/0012-821X(92)90175-U.

Thomson, R.E., S.F. Mihaly, A.B. Rabinovich, R.E. McDuff, S.R. Veris, and F.R. Stahr. 2003. Constrained circulation at Endeavour

ridge facilitates colonization by vent larvae. *Nature* 424:545–549, http://dx.doi.org/10.1038/nature01824.

Thomson, R.E., M.M. Subbotina, and M.V. Anisimov. 2005. Numerical simulation of hydrothermal vent-induced circulation at Endeavour Ridge. *Journal of Geophysical Research* 110, C01004, http://dx.doi.org/10.1029/2004JC002337.

Tivey, M.K. 2007. Generation of seafloor hydrothermal vent fluids and associated mineral deposits. *Oceanography* 20(1):50-65, http://dx.doi.org/10.5670/oceanog.2007.80.

Tolstoy, M., F. Waldhauser, D.R. Bohnenstiehl, R.T. Weekly, and W.-Y. Kim. 2008. Seismic identification of along-axis hydrothermal flow on the East Pacific Rise. *Nature* 451:181–184, http://dx.doi.org/10.1038/nature06424.

Turner, J.S., and I.H. Campbell. 1987. Temperature, density and buoyancy fluxes in "black smoker" plumes, and the criterion for buoyancy reversal. *Earth and Planetary Science Letters* 86:85–92, http://dx.doi.org/10.1016/0012-821X(87)90191-9.

Van Ark, E.M., R.S. Detrick, J.P. Canales, S.M. Carbotte, A.J. Harding, G.M. Kent, M.R. Nedimovic, W.S.D. Wilcock, J.B. Diebold, and J.M. Babcock. 2007. Seismic structure of the Endeavour Segment, Juan de Fuca Ridge: Correlations with seismicity and hydrothermal activity. *Journal of Geophysical Research* 112, B02401, http://dx.doi.org/10.1029/2005JB004210.

Veirs, S.R., R.E. McDuff, and F.R. Stahr. 2006. Magnitude and variance of near-bottom horizontal heat flux at the Main Endeavour hydrothermal vent field. *Geochemistry Geophysics Geosystems* 7, Q02004, http://dx.doi.org/10.1029/2005GC000952.

Von Damm, K.L., and M.D. Lilley. 2004. Diffuse flow hydrothermal fluids from 9°50'N East Pacific Rise: Origin, evolution and biogeochemical controls. Pp. 245–268 in *The Subseafloor Biosphere at Mid-Ocean Ridges*. W.S.D. Wilcock E.F. DeLong, D.S. Kelley, J.A. Baross, and S.C. Cary, eds, Geophysical Monograph Series, vol. 144, American Geophysical Union, Washington, DC.

Webster, H., and D. Thomson. 2002. Validation of a Lagrangian model plume rise scheme using the Kincaid data set. *Atmospheric Environment* 36:5,031–5,042, http://dx.doi.org/10.1016/S1352-2310(02)00559-9.

Woods, A.W., and J.R. Delaney. 1992. The heat and fluid transfer associated with the flanges on hydrothermal venting structures. *Earth and Planetary Science Letters* 112:117–129, http://dx.doi.org/10.1016/S0012-821X(97)00137-4.

Xu, G., and D. Di Iorio. 2011. The relative effects of particles and turbulence on acoustic scattering from deep-sea hydrothermal vent plumes. *Journal of the Acoustical Society of America* 130:1,856–1,867.